

hep-ph/9507413
TUM-HEP-223/95
Revised version:
To appear in PRD

Large uncertainties in the cross section of elastic $W_L^+W_L^-$ scattering

Kurt Riesselmann*

*Physik-Department T30, Technische Universität München,
James-Frank-Straße, 85747 Garching b. München, Germany*

Abstract

The Standard Model amplitudes for $2 \rightarrow 2$ scattering processes involving longitudinally polarized gauge bosons (W_L^\pm, Z_L) and the Higgs boson are analyzed up to two loops. Assuming $M_H \gg M_W$, the trilinear Higgs coupling, λv , is dominant for energies of $\sqrt{s} < 1.5 - 2 M_H$. For larger values of \sqrt{s} , the quartic coupling, λ , becomes dominant, allowing for a simpler calculation of higher-order corrections. The resulting high-energy amplitudes display a large logarithmic dependence on \sqrt{s} which can be resummed using renormalization group techniques. For $M_H < 350$ GeV, a next-to-leading-log calculation is sufficient. For $350 < M_H < 450$ GeV, a next-to-next-to-leading-log calculation is necessary to include large two-loop corrections. For a Higgs mass larger than $O(450 \text{ GeV})$ and $\sqrt{s} > 2M_H$, the perturbative results are not reliable. Choosing the $\overline{\text{MS}}$ renormalization scheme instead of the OMS scheme, the coefficients of the perturbative series increase in magnitude, making the breakdown of perturbation theory even more apparent. In conclusion, the perturbative cross sections presented here show very large uncertainties if $M_H \gtrsim 450$ GeV and $\sqrt{s} \gtrsim 2M_H$, reducing the sensitivity to contributions from new physics significantly.

PACS number(s): 14.80.Bn, 14.70.Fm, 11.10.Jj

Typeset using REVTeX

*Electronic address: kurtr@physik.tu-muenchen.de

I. INTRODUCTION

In the Standard Model, the weak gauge bosons W^\pm and Z acquire a mass by means of the Higgs mechanism [1]. Though the masses M_W and M_Z are experimentally well-known, the Higgs particle itself has not yet been observed. This leaves the Higgs mass to be the last undetermined parameter of the Standard Model. Knowing the Higgs mass, M_H , the Higgs quartic coupling, $\lambda = G_F M_H^2/\sqrt{2}$, and the Higgs trilinear coupling, $\lambda v = G_F^{1/2} M_H^2/8^{1/4}$, are fixed. All three quantities are intimately connected to the scattering of longitudinally polarized gauge bosons W_L^\pm and Z_L : The Higgs mass corresponds to the pole of the cross section, and the Higgs couplings present the dominant contributions to the cross section if $M_H \gg M_W$. To test the Standard Model Higgs sector, it is therefore important to analyze the cross sections of elastic $2 \rightarrow 2$ processes involving longitudinally polarized gauge bosons and the Higgs boson in more detail. Only if we understand the Standard Model scattering processes we are able to test the Higgs couplings phenomenologically. Large uncertainties in the Standard Model cross sections decrease the experimental sensitivity to new physics significantly.

Assuming $\sqrt{s}, M_H \gg M_W$, we discuss the amplitudes for $2 \rightarrow 2$ scattering processes involving longitudinally polarized gauge bosons (W_L^\pm, Z_L) and the Higgs boson. We briefly review the one-loop results and examine the validity of the high-energy approximation. We present the two-loop high-energy amplitudes, and find both the logarithmic and the non-logarithmic corrections to be important if M_H is large. Using renormalization group techniques, the logarithms are resummed including the complete set of next-to-next-to-leading logarithms (NNLL). This gives a perturbative series in the running coupling. We find the perturbative character of this series to break down if $M_H \gtrsim 450$ GeV and $\sqrt{s} \gtrsim 2M_H$.

II. FRAMEWORK

For electroweak processes in which both $\sqrt{s} \gg M_W$ and $M_H \gg M_W$, the electroweak interactions are dominated by the coupling of the longitudinal components of the vector bosons, W_L^\pm, Z_L , to each other and to other particles (leptons, quarks, or Higgs particle). This is known as the equivalence theorem (EQT) [2,3]. In this limit, the dominant coupling constants are the Higgs quartic coupling λ , the Higgs trilinear coupling λv , and the Yukawa couplings of the heavy fermions. The quantity v is the vacuum expectation value of the Higgs sector, $v = 2^{-1/4} G_F^{-1/2} = 246$ GeV. Choosing the appropriate renormalization scheme [4], the subdominant electroweak gauge couplings can be neglected. Setting $g_1 = g_2 = 0$, the longitudinal components of the electroweak gauge bosons can be identified as the three massless Goldstone bosons, w^+, w^- , and z of the Higgs sector. In this limit, all interactions are determined by the Lagrangian

$$\mathcal{L}_{\text{EQT}} = \mathcal{L}_H + \mathcal{L}_F, \quad (2.1)$$

where \mathcal{L}_H is the Lagrangian of the Higgs sector and describes the interactions of the four scalar particles H, w^+, w^- , and z among each other, and \mathcal{L}_F is the fermionic Lagrangian which describes the Yukawa interactions between the four scalar particles and the fermions of the theory.

In our investigation of the high energy behaviour of longitudinally polarized gauge boson and Higgs boson scattering, we neglect the fermionic contributions and concentrate on the physics determined by \mathcal{L}_H :

$$\mathcal{L}_H = \frac{1}{2}(\partial_\mu \Phi)^\dagger (\partial^\mu \Phi) - \frac{\lambda}{4}(\Phi^\dagger \Phi)^2 + \frac{\mu^2}{2}(\Phi^\dagger \Phi). \quad (2.2)$$

Here Φ is a complex doublet. After writing Φ in terms of real scalar fields and introducing a vacuum expectation value (vev) for one of the fields, we obtain the SM interactions:

$$\mathcal{L}_{int} = -\frac{\lambda}{4}(\mathbf{w}^4 + 2\mathbf{w}^2 H^2 + H^4) - \lambda v(\mathbf{w}^2 H + H^3), \quad (2.3)$$

where $\mathbf{w} = (w^+, w^-, z)$. The quartic interactions by themselves satisfy a $\text{SO}(4)$ symmetry, whereas the whole interaction Lagrangian is only $\text{SO}(3)$ symmetric [6]. These symmetries will reappear when discussing the scattering amplitudes.

Note that \mathcal{L}_{int} does not provide for trilinear couplings of the Goldstone bosons. Correspondingly, the trilinear gauge couplings of the Standard Model are pure gauge couplings and are not subject of our analysis.

III. OMS AND $\overline{\text{MS}}$ RENORMALIZATION

The Lagrangian \mathcal{L}_H must be renormalized under the constraint that the Goldstone bosons remain massless at all orders of perturbation theory, i.e., the Goldstone theorem [5] applies. Equivalently, we require the Higgs field to be expanded around the minimum of the potential, acquiring a vacuum expectation value of $v = 2^{-1/4} G_F^{-1/2} \approx 246$ GeV. We use dimensional regularization, so that the requirement above leads to the relation [7]

$$\lambda_0 = \frac{M_0^2}{Z_w M_H^2} \lambda. \quad (3.1)$$

Here λ_0 (λ) is the bare (renormalized) quartic coupling, Z_w is the field renormalization constant of the charged Goldstone bosons, and M_0 (M_H) is the bare (renormalized) Higgs mass. Note that Eq. (3.1) is *renormalization scheme independent*. In the limit of zero Yukawa couplings, $Z_w = Z_z$ due to the $\text{SO}(3)$ symmetry of \mathcal{L}_H .

In the OMS scheme, the explicit two-loop expressions for λ_0 , Z_w , and M_0 are given in [7], and the necessary expressions for the self-energies and wave-function renormalizations have also been reported in [8]. In this scheme, the mass M_H is defined as the pole mass, i.e., the physical mass of the Higgs boson. Counterterms are defined such that the value of M_H remains unchanged when going to higher orders in perturbation theory. In other words, the pole of the Higgs propagator is always at the physical mass M_H . Similarly, the OMS scheme fixes the vacuum expectation value v to have the same value at each order. Hence, the tree level relation

$$\lambda_{\text{OMS}} = \frac{M_H^2}{2v^2} \quad (3.2)$$

is unchanged by higher-order corrections. Therefore, the OMS-value of the Higgs coupling, λ_{OMS} , is given by Eq. (3.2) to *all orders* in perturbation theory.

In the $\overline{\text{MS}}$ scheme, we find the following results:

$$Z_w = Z_H = 1 + \frac{\lambda_{\overline{\text{MS}}}^2 \xi^{2\epsilon}}{(16\pi^2)^2} \left(-\frac{3}{\epsilon} \right) + \text{O}(\lambda_{\overline{\text{MS}}}^3), \quad (3.3)$$

$$\lambda_0 = \lambda_{\overline{\text{MS}}} \left[1 + \frac{\lambda_{\overline{\text{MS}}} \xi^\epsilon}{16\pi^2} \left(\frac{12}{\epsilon} \right) + \frac{\lambda_{\overline{\text{MS}}}^2 \xi^{2\epsilon}}{(16\pi^2)^2} \left(\frac{144}{\epsilon^2} - \frac{78}{\epsilon} \right) + \text{O}(\lambda_{\overline{\text{MS}}}^3) \right], \quad (3.4)$$

$$M_0^2 = \overline{M}^2 \left[1 + \frac{\lambda_{\overline{\text{MS}}} \xi^\epsilon}{16\pi^2} \left(\frac{12}{\epsilon} \right) + \frac{\lambda_{\overline{\text{MS}}}^2 \xi^{2\epsilon}}{(16\pi^2)^2} \left(\frac{144}{\epsilon^2} - \frac{81}{\epsilon} \right) + \text{O}(\lambda_{\overline{\text{MS}}}^3) \right], \quad (3.5)$$

where $\epsilon = (4 - D)/2$, D is the dimensionality of space-time, and $\xi = 4\pi e^{-\gamma_E}$, with $\gamma_E = 0.5772\dots$ the Euler constant. The $\overline{\text{MS}}$ Higgs mass is denoted as \overline{M} .

Knowing the bare coupling λ_0 in terms of both the OMS coupling and the $\overline{\text{MS}}$ coupling, we can calculate the relation between $\lambda_{\overline{\text{MS}}}$ and λ_{OMS} order by order in perturbation theory. Up to two loops we find:

$$\begin{aligned} \lambda_{\overline{\text{MS}}}(\mu_0) = \lambda_{\text{OMS}} & \left[1 + \left(12 \ln(\mu_0^2/M_H^2) + 25 - 3\pi\sqrt{3} \right) \frac{\lambda_{\text{OMS}}}{16\pi^2} \right. \\ & + \left(144 \ln^2(\mu_0^2/M_H^2) + (444 - 72\pi\sqrt{3}) \ln(\mu_0^2/M_H^2) + 524\zeta(2) \right. \\ & \quad \left. - 90\zeta(3) + 216\sqrt{3}\mathbf{Cl} - 225\pi\sqrt{3} + 48\pi\mathbf{Cl} + 162K_5 + 75 \right) \frac{\lambda_{\text{OMS}}^2}{(16\pi^2)^2} \\ & \left. + \text{O}(\lambda_{\text{OMS}}^3) \right], \end{aligned} \quad (3.6)$$

$$\begin{aligned} \approx \lambda_{\text{OMS}} & \left[1 + \left(12 \ln(\mu_0^2/M_H^2) + 8.676 \right) \frac{\lambda_{\text{OMS}}}{16\pi^2} \right. \\ & + \left(144 \ln^2(\mu_0^2/M_H^2) + 52.219 \ln(\mu_0^2/M_H^2) + 286.836 \right) \frac{\lambda_{\text{OMS}}^2}{(16\pi^2)^2} \\ & \left. + \text{O}(\lambda_{\text{OMS}}^3) \right], \end{aligned} \quad (3.7)$$

where M_H is the physical Higgs mass, and μ_0 is the arbitrary mass scale in dimensional regularization. The constant $K_5 = 0.92363\dots$ was evaluated numerically in [7]. The Riemann ζ function takes the values $\zeta(2) = \pi^2/6$ and $\zeta(3) = 1.20205\dots$, \mathbf{Cl} is the maximum of Clausen's function, $\mathbf{Cl} \equiv \text{Cl}(\frac{\pi}{3}) = 1.01494\dots$. The two-loop constant (286.836...) contains contributions from the one-loop $\text{O}(\epsilon)$ term of the bare coupling in the OMS scheme. Note that the coefficients of the n -loop logarithmic terms, $\ln^m(\mu_0^2/M_H^2)$, $1 \leq m \leq n$, can also be determined using the coefficients of the n -loop beta function in connection with the $(n-1)$ -loop result. To one loop, our expression agrees with the result by Sirlin and Zucchini [9]. For a further discussion we refer to [10].

Because the OMS-coupling is entirely fixed by the choice of the physical Higgs mass, M_H , the $\overline{\text{MS}}$ coupling is now entirely fixed by the choice of the scale μ_0 and the value of M_H . We make the natural choice $\mu_0 = M_H$ when using the $\overline{\text{MS}}$ coupling. This choice also guarantees that all higher-order logarithmic terms do not contribute to the correction.

IV. SCATTERING AMPLITUDES

We are now able to carry out our analysis of $2 \rightarrow 2$ scattering processes involving longitudinally polarized gauge bosons and the Higgs boson in the limit $\sqrt{s}, M_H \gg M_W$. We neglect gauge and Yukawa couplings, and use the EQT as explained above. First, we briefly review the exact EQT one-loop results [11,12], and compare them with the corresponding high-energy, $\sqrt{s} \gg M_H \gg M_W$, one-loop results obtained by [13–15]. This establishes the range of validity of the high-energy approximation. Next, we consider the limit of high-energy scattering at two loops. The latter calculation yields the information necessary to carry out a RGE analysis up to next-to-next-to-leading logarithms, NNLL. We investigate both the OMS- and the $\overline{\text{MS}}$ -scheme.

The Feynman diagrams needed for the scattering processes are determined by the interaction Lagrangian of Eq. (2.3). The relevant couplings are the quartic coupling λ and the trilinear coupling λv , see Fig. 1. We consider all possible two-body initial and final states with total charge equal zero: $W_L^+ W_L^-$, $Z_L Z_L$, HH , $Z_L H$; in the notation of massless Goldstone bosons: $w^+ w^-$, zz , HH , zH . Because of the $\text{SO}(3)$ symmetry of the Lagrangian \mathcal{L}_H , we can write the unrenormalized transition amplitudes in terms of three different functions A' , A'' , A''' , each depending on the Mandelstam variables s, t, u . Taking the two-body channels in the order $w^+ w^-$, zz , HH , zH , the 4×4 matrix of the unrenormalized transition amplitudes, \mathcal{F} , is given by [15]

$$\mathcal{F} = \begin{pmatrix} A'(s) + A'(t) & A'(s) & A''(s) & 0 \\ A'(s) & A'(s) + A'(t) + A'(u) & A''(s) & 0 \\ A''(s) & A''(s) & A'''(s) + A'''(t) + A'''(u) & 0 \\ 0 & 0 & 0 & A''(t) \end{pmatrix}, \quad (4.1)$$

where we have indicated only the first variable in the functions A since these functions are unchanged by an interchange of the remaining two variables: For example, $A'(t) \equiv A'(t, s, u) = A'(t, u, s)$. The channels $W_L^+ W_L^- \rightarrow W_L^+ W_L^-$ and $H Z_L \rightarrow H Z_L$ are the only channels that do not display a $t \leftrightarrow u$ symmetry in their amplitudes.

To obtain finite and physical S -matrix elements, we need to multiply the unrenormalized amplitudes by the wavefunction renormalization constants of the external fields, including finite parts such that the residue of the external propagators is equal to unity.¹ The physical transition amplitude is then

$$\mathcal{M} = \mathbf{Z} \mathcal{F} \mathbf{Z}, \quad (4.2)$$

where \mathbf{Z} is a diagonal matrix of renormalization constants,

$$\mathbf{Z} = \text{diag}(Z_w, Z_w, Z_H, Z_H^{1/2} Z_w^{1/2}). \quad (4.3)$$

For a consistent calculation, the products in \mathcal{M} are to be expanded to $\mathcal{O}(\lambda^3)$, dropping higher orders.

¹In the OMS scheme this is done by definition. In the $\overline{\text{MS}}$ scheme, additional finite wavefunction renormalization constants need to be taken into account [17].

At high energies, $\sqrt{s} \gg M_H$, all internal particles of the scattering diagrams can be taken massless. Hence, the Feynman diagrams only depend on \sqrt{s} , λ , λv , and the scattering angle. Because of the even number of external particles, the trilinear coupling, λv , must always enter the $2 \rightarrow 2$ Feynman diagrams in even powers. Furthermore, $(\lambda v)^2 = M_H^2 \lambda [1 + \mathcal{O}(\lambda)]/2$ in any renormalization scheme. Using dimensional arguments we conclude that Feynman scattering diagrams involving trilinear couplings are suppressed by powers of M_H^2/s relative to those which contain only quartic couplings. To illustrate this point, we look at the tree-level result for $W_L^+ W_L^- \rightarrow Z_L Z_L$:

$$A'(s, t, u) = -2\lambda - \frac{4\lambda^2 v^2}{s - M_H^2} + \mathcal{O}(\lambda^2) + \mathcal{O}(\lambda^4 v^4) \quad (4.4)$$

$$= -2\lambda \left(1 + \frac{M_H^2}{s - M_H^2} \right) + \mathcal{O}(\lambda^2) + \mathcal{O}(\lambda^2 M_H^2) \quad (4.5)$$

$$\xrightarrow{s \gg M_H^2} -2\lambda + \mathcal{O}(\lambda^2) + \mathcal{O}\left(\frac{M_H^2}{s}\right). \quad (4.6)$$

Neglecting the trilinear couplings, the interaction Lagrangian, Eq. (2.3), becomes $\text{SO}(4)$ -symmetric, and so do the high energy Feynman amplitudes. That is,

$$\lim_{s \gg M_H^2} A'(s) = \lim_{s \gg M_H^2} A''(s) = \lim_{s \gg M_H^2} A'''(s) \equiv A(s), \quad (4.7)$$

thus simplifying the scattering amplitudes significantly.

The physical scattering amplitude \mathcal{M} , however, has no $\text{SO}(4)$ symmetry, since the renormalization constants Z_w and Z_H are defined at the renormalization points $p^2 = 0$ and $p^2 = M_H^2$, respectively. Therefore, they contain contributions involving trilinear couplings, breaking the $\text{SO}(4)$ symmetry. In addition, the Higgs mass has to be kept non-zero when calculating self-energies and renormalization constants. This introduces a logarithmic dependence of the high-energy S -matrix elements on M_H , despite the fact that the Higgs mass occurring inside Feynman diagrams is set to zero.

It is of interest to know for which energies \sqrt{s} the high-energy approximation can be used. Looking at Eq. (4.5), we expect the difference of the exact and high-energy results to be of the order $M_H^2/(s - M_H^2)$. For example, the choice $\sqrt{s} \approx 3M_H$ is expected to give an error of 10 to 15% in magnitude. We examine whether this changes at the one-loop level by comparing the exact one-loop EQT result with the high-energy EQT result in the OMS scheme.

A. OMS amplitudes

The exact one-loop renormalized transition amplitudes including both quartic and trilinear Higgs coupling contributions are taken from Eqs. (3.5)–(3.7) of [12] and were also calculated in [11]. The high energy result, $\sqrt{s} \gg M_H$, is obtained by dropping scattering diagrams involving the trilinear coupling λv and setting the Higgs mass of internal Higgs propagators equal to zero. The resulting high-energy amplitudes agree with the one-loop high-energy results reported in [13–15]. We also present the two-loop high-energy amplitudes which we calculate using the results of [7].

Since the matrix elements depend on the scattering angle, we integrate out this angular dependence and compare partial-wave projected $2 \rightarrow 2$ amplitudes for angular momentum j . They are defined by [15]

$$\mathbf{a}_j^{if}(s) = \frac{N_i N_f}{32\pi} \left(\frac{4|\vec{p}_i||\vec{p}_f|}{s} \right)^{1/2} \int_{-1}^1 d(\cos \theta) \mathcal{M}^{if}(s, \cos \theta) P_j(\cos \theta). \quad (4.8)$$

The momentum-dependent prefactor approaches unity for $\sqrt{s} \gg M_H$. The factors N_i, N_f incorporate the symmetry factors which must be inserted for each pair of identical particles in the initial and final state, $N_i, N_f = 1/\sqrt{2}$ for zz, HH , and $N_i, N_f = 1$ for w^+w^-, zH .

To discuss the validity of the high-energy approximation, we explicitly state the result for the channel $W_L W_L \rightarrow Z_L Z_L$. The analytical result of this specific channel is given in Appendix A. Numerical evaluation yields the following OMS high-energy amplitude up to two loops:

$$\begin{aligned} W_L^+ W_L^- \rightarrow Z_L Z_L : \quad & \text{OMS scheme} \\ \mathbf{a}_{j=0}(s) = & \frac{N_i N_f}{32\pi} \left(\frac{4|\vec{p}_i||\vec{p}_f|}{s} \right)^{1/2} (-4 \lambda_{\text{OMS}}) \left[1 \right. \\ & + \left[12 \ln \left(\frac{s}{M_H^2} \right) - 21.32 - 25.13 i \right] \frac{\lambda_{\text{OMS}}}{16\pi^2} \\ & + \left[144 \ln^2 \left(\frac{s}{M_H^2} \right) - (655.8 + 603.2 i) \ln \left(\frac{s}{M_H^2} \right) \right. \\ & \left. \left. + 684.4 + 1097.0 i \right] \frac{\lambda_{\text{OMS}}^2}{(16\pi^2)^2} \right]. \end{aligned} \quad (4.9)$$

Notice that the tree-level high-energy amplitude is independent of s since the kinematical prefactor is evaluated to be one. The tree-level result is therefore not an adequate description of the high-energy amplitude if using λ_{OMS} .

In Fig. 2 we show the OMS $j = 0$ partial-wave projected amplitudes² of the channel $W_L^+ W_L^- \rightarrow Z_L Z_L$, giving the high-energy EQT result at tree and one-loop level, and comparing them with the corresponding tree and one-loop results of the exact EQT calculation. In addition, we also show the high-energy two-loop result. These results are compared for both $M_H = 200$ (left plot) and 500 GeV (right plot). Note that the amplitude scale is a factor 10 different in the two plots. This is necessary since the Higgs coupling λ_{OMS} increases a factor of 6.25 when going from $M_H = 200$ to $M_H = 500$ GeV.

We show $\text{Re} a_{j=0}$ only for values $\sqrt{s} > M_H$. (For values of $\sqrt{s} < M_H$, the real part becomes positive and is not shown.) The exact EQT result features the typical pole [16] at $\sqrt{s} = M_H$, whereas the high-energy amplitude remains finite at the pole location. Increasing \sqrt{s} , the exact result approaches the high-energy result rather quickly, confirming

²The $2 \rightarrow 2$ processes considered here are predominantly s -wave processes, so that only $j = 0$ is of interest. For $W_L^+ W_L^- \rightarrow Z_L Z_L$, the $j = 1$ amplitude is zero, and the $j = 2$ amplitude is suppressed roughly by a factor of 100.

the suppression of the trilinear coupling contributions at higher energies. We find that for values $\sqrt{s} > 3M_H$, the relative difference

$$\Delta(a_{j=0}) = \frac{a_{j=0}^{\text{exact}} - a_{j=0}^{\text{high}}}{a_{j=0}^{\text{exact}}} \quad (4.10)$$

between the exact and high-energy EQT result is less than 12% at tree level. However, taking higher order corrections into account, the relative difference increases. The heavy-Higgs case shows a larger difference than the light-Higgs case when keeping \sqrt{s}/M_H fixed. This is due to the fact that a larger Higgs mass also causes a larger Higgs coupling, increasing the importance of higher-order corrections. In Table I we show the relative differences for three different values of M_H and a range of \sqrt{s} . Choosing $M_H < 500$ GeV the error induced by using the high-energy approximation is less than approximately 20% if $\sqrt{s} \gtrsim 3M_H$. For such cms-energies, the numerical difference between different orders in perturbation theory (e.g. tree-level vs. one-loop) is much more significant than the difference between exact EQT and high-energy EQT result.

It is also interesting to note that for $\sqrt{s} \approx 1.5M_H$ the high-energy result contributes about 50% to the real part of the $j = 0$ partial-wave projected amplitude, i.e., the quartic coupling becomes dominant. Since it is desirable to measure the quartic coupling λ and the trilinear coupling λv separately, the two different contributions to the cross section need to be separated. This only seems feasible by going to the high-energy region in which the trilinear coupling is completely suppressed. Since the cross sections decrease quickly for $\sqrt{s} > M_H$ this is a difficult task. If the quartic coupling can be measured at high energies ($\sqrt{s} \approx 3 - 5M_H$), one can extrapolate the high-energy cross section back to $\sqrt{s} \approx M_H$. Subtracting the quartic coupling contribution from the cross section at the resonance would yield the pure trilinear contribution at the resonance. To do the extrapolation from high energies to resonance energies, the behaviour of the high-energy amplitude as a function of \sqrt{s} has to be well understood. This will be the subject of Section V, where we introduce RGE methods. Before doing so, we briefly state the results of the high-energy amplitudes when using the $\overline{\text{MS}}$ scheme.

B. $\overline{\text{MS}}$ AMPLITUDES

The high-energy $\overline{\text{MS}}$ amplitudes are calculated in two different ways. One way to obtain the amplitudes is to calculate the high-energy Feynman diagrams, taking all particles to be massless. The result is renormalized using the $\overline{\text{MS}}$ definitions for the bare coupling and the wavefunction renormalization constant, Eqs. (3.3) and (3.4). Finally, the physical transition amplitude is obtained by multiplying the renormalized four-point functions with the finite renormalization constants of the external fields [17].

Alternatively, the $\overline{\text{MS}}$ transition amplitudes can also be calculated by taking the result of the OMS amplitudes and expressing the OMS coupling in terms of the $\overline{\text{MS}}$ coupling by means of Eq. (3.6). The quantity M_H appearing in the final amplitudes refers to the pole mass of the Higgs propagator, *not* the $\overline{\text{MS}}$ mass.

Again choosing the specific channel $W_L W_L \rightarrow Z_L Z_L$, the $\overline{\text{MS}}$ partial-wave projected amplitude in the high-energy limit is:

$W_L^+ W_L^- \rightarrow Z_L Z_L$: $\overline{\text{MS}}$ scheme

$$\begin{aligned} \mathbf{a}_{j=0}(s) = & \frac{N_i N_f}{32\pi} \left(\frac{4|\vec{p}_i||\vec{p}_f|}{s} \right)^{1/2} \left(-4 \lambda_{\overline{\text{MS}}}(\mu_0) \right) \left[1 \right. \\ & + \left[12 \ln \left(\frac{s}{\mu_0^2} \right) - 30.000 - 25.13 i \right] \frac{\lambda_{\overline{\text{MS}}}(\mu_0)}{16\pi^2} \\ & + \left[144 \ln^2 \left(\frac{s}{\mu_0^2} \right) - (876.0 + 603.2 i) \ln \left(\frac{s}{\mu_0^2} \right) + 12 \ln \left(\frac{s}{M_H^2} \right) \right. \\ & \left. \left. + 918.1 + 1533.1 i \right] \frac{[\lambda_{\overline{\text{MS}}}(\mu_0)]^2}{(16\pi^2)^2} \right]. \end{aligned} \quad (4.11)$$

At each order, the leading terms in $\ln(s)$ have the same coefficients as in the OMS scheme, see Eq. (4.9). The difference is in the constant terms which also lead to different coefficients for the subleading logarithms. The scale μ_0 is the scale at which the Higgs $\overline{\text{MS}}$ coupling is defined, and its natural value is of the order of the Higgs mass, $\mu_0 \approx M_H$.

The $\ln(s/M_H^2)$ term of the $\overline{\text{MS}}$ result is due to the finite wavefunction renormalization of the external fields which enter the physical transition amplitudes. The wavefunction renormalizations are low-energy quantities. At one-loop, $Z_w = Z_z$ is finite, and no $\ln(M_H)$ terms occur. At two loops, Z_w is divergent, and the finite pieces of the wavefunction renormalization constants provide for a $\ln(M_H)$ dependence.

The result of the previous equation can be compared with the OMS amplitudes of Eq. (4.9). We find that the $\overline{\text{MS}}$ constants are larger than the corresponding OMS quantities. Evaluating the $\overline{\text{MS}}$ coupling for $\mu_0 = M_H$, we find that $\lambda_{\overline{\text{MS}}}(M_H)$ is larger than λ_{OMS} . Hence *both* the coefficients *and* the coupling are larger than the corresponding quantities of the OMS scheme, resulting in larger radiative corrections. A similar effect is observed in the $\mathcal{O}(\lambda^2)$ corrections in the Higgs decays $H \rightarrow f\bar{f}$ [18,19,10] and $H \rightarrow W^+W^-$ [10]. A more detailed discussion of the $\overline{\text{MS}}$ amplitudes is provided at the end of the following section.

V. RENORMALIZATION GROUP METHODS

The previous section provided the amplitudes as obtained from calculating Feynman diagrams to a certain order in perturbation theory. Using renormalization group techniques, we are also able to resum the energy dependence of the amplitudes at higher orders. In the context of weak gauge boson scattering this was originally introduced by [13–15] at the one-loop level.

The amplitudes are subject to renormalization group equations. Using the OMS scheme, the high-energy transition amplitude must satisfy the homogenous Callan-Symanzik equation [20]:

$$\left[M_H \frac{\partial}{\partial M_H} + \beta(\lambda_{\text{OMS}}) \frac{\partial}{\partial \lambda_{\text{OMS}}} - \sum_{i=1}^4 \gamma_i \right] \mathbf{a}_j = 0. \quad (5.1)$$

This equation is only valid in the high-energy region. At low energies, the right-hand-side of the equation is replaced by an inhomogenous term.

Using the $\overline{\text{MS}}$ scheme, the transition amplitude must satisfy the 't Hooft-Weinberg-equation [21]:

$$\left[\mu \frac{\partial}{\partial \mu} + \bar{\beta}(\lambda_{\overline{\text{MS}}}) \frac{\partial}{\partial \lambda_{\overline{\text{MS}}}} - \bar{\gamma}_M(\lambda_{\overline{\text{MS}}}) \overline{M} \frac{\partial}{\partial \overline{M}} \right] \mathbf{a}_j = 0, \quad (5.2)$$

where \overline{M} is the scale-dependent $\overline{\text{MS}}$ mass. This differential equation is exact at all energies. We will now solve the RGE and discuss the RG improved amplitudes and cross sections in both schemes.

A. RGE in OMS scheme

The physical meaning of the homogenous Callan-Symanzik-equation, Eq. (5.1), can be stated as follows: If all momenta are scaled by a factor σ so that $s, t, u \rightarrow \sigma^2 s, \sigma^2 t, \sigma^2 u$, the scaled and original $2 \rightarrow 2$ scattering amplitudes are related by [22]

$$\mathcal{M}(\{\sigma p_i\}, \lambda, M_H) = \Gamma_{i_1} \Gamma_{i_2} \mathcal{M}(\{p_i\}, \lambda_s(\sigma), M_H) \Gamma_{f_1} \Gamma_{f_2}. \quad (5.3)$$

The Γ_ϕ are related to the field anomalous dimensions of the Higgs sector:

$$\Gamma_\phi = \exp \left(- \int_{\lambda_s(1)}^{\lambda_s(\sigma)} \frac{\gamma_\phi(\lambda)}{\beta(\lambda)} d\lambda \right), \quad \phi = w^\pm, z, H, \quad (5.4)$$

and $\lambda_s(\sigma)$ is the OMS running coupling. The functions β and γ_ϕ are the usual Callan-Symanzik renormalization group functions, in particular:

$$\beta(\lambda) \equiv \mu \frac{d\lambda}{d\mu} \equiv \frac{\beta_0}{16\pi^2} \lambda^2 + \frac{\beta_1}{(16\pi^2)^2} \lambda^3 + \frac{\beta_2}{(16\pi^2)^2} \lambda^4 + \mathcal{O}(\lambda^5). \quad (5.5)$$

The OMS coefficients of the β function have been calculated to three loops [23,10]:

$$\beta_0 = 24, \quad \beta_1 = -312, \quad \beta_2^{\text{OMS}} = 4238.23 \dots \quad (5.6)$$

The values of β_0 and β_1 are scheme independent. The three-loop coefficient β_2 is scheme dependent, and its value given above refers to the OMS scheme. The field anomalous dimensions of the three Goldstone bosons are identical and will be denoted as γ_w . At one loop, γ_w and γ_H are zero. At two loops, their value is scheme dependent. In the OMS scheme they are [25]

$$\gamma_w(\lambda) = \gamma_{w,0} \frac{\lambda^2}{(16\pi^2)^2} + \mathcal{O}(\lambda^3), \quad \gamma_{w,0} = -6, \quad (5.7)$$

$$\gamma_H(\lambda) = \gamma_{H,0} \frac{\lambda^2}{(16\pi^2)^2} + \mathcal{O}(\lambda^3), \quad \gamma_{H,0} = (150 - 24\pi\sqrt{3}) \approx 19.41 \dots \quad (5.8)$$

The solution of the differential equation, Eq. (5.5), defines the running coupling λ_s . Rewriting the parameter σ as μ/μ_0 we have

$$\ln(\mu/\mu_0) = \int_{\lambda_s(1)}^{\lambda_s(\mu/\mu_0)} \frac{d\lambda}{\beta(\lambda)}. \quad (5.9)$$

This equation can be solved for $\lambda_s(\mu/\mu_0)$ iteratively, assuming the expansion parameter $\lambda(\mu_0)$ to be small, i.e., perturbation theory to be valid. Then the differential equation of the running coupling can be solved iteratively and the two-loop answer is

$$\lambda_s^{(2)}(\mu/\mu_0) = \lambda_s(1) \left[1 - \beta_0 \hat{\lambda}_s(1) \ln\left(\frac{\mu}{\mu_0}\right) + \frac{\beta_1}{\beta_0} \hat{\lambda}_s(1) \ln\left(1 - \beta_0 \hat{\lambda}_s(1) \ln\left(\frac{\mu}{\mu_0}\right)\right) \right]^{-1} \quad (5.10)$$

where $\hat{\lambda}_s \equiv \lambda_s/(16\pi^2)$. The superscript (2) indicates that this expression is the two-loop running coupling. The iterative solution for the three-loop running coupling $\lambda_s^{(3)}$ is given in [10], together with a discussion of other perturbative solutions for the running coupling.

The running coupling of a given renormalization scheme depends only on the value of the Higgs quartic coupling at the scale $\mu = \mu_0$, i.e. $\lambda_s(1)$. In the OMS scheme, we take $\mu_0 = M_H$ and choose $\lambda_s(1)$ to be equal to the non-running coupling λ_{OMS} :

$$\lambda_s(1) = \lambda_{\text{OMS}} = \frac{M_H^2}{2v^2} = \frac{G_\mu M_H^2}{\sqrt{2}}. \quad (5.11)$$

The evolution of the transition amplitude when going from the scale $\mu = \mu_0 \equiv M_H$ to the scale $\mu = \sqrt{s}$ is now determined by the evolution of the running coupling. In Fig. 3 we show the running coupling $\lambda_s(\sqrt{s}/M_H)$ at one, two, and three loops. For each value of M_H we show the value of $\lambda_s(1)$, i.e. $\sqrt{s} = M_H$ (dotted curve), and the value of the running coupling at $\sqrt{s} = 4000$ GeV. Requiring that the two-loop and one-loop coupling differ by less than 50% for $M_H \leq \sqrt{s} \leq 4000$ GeV, the Higgs mass should be less than 500 GeV.³ As we will see below, this value of M_H is still too large for a perturbative RG treatment of high-energy amplitudes and cross sections.

We are now able to estimate the importance the logarithms. If $\sqrt{s} \gg M_H$ they are expected to be very important. The question is: When is \sqrt{s} large? To get a first estimate we look at the denominator of the running coupling, Eq. (5.10), at one loop. With the above choices of μ and μ_0 , it is given by $1 - 24 \ln(\sqrt{s}/M_H) M_H^2/(32\pi^2 v^2)$. We expect to approach the nonperturbative region if this quantity is about 0.5; in other words, if the one-loop running coupling $\lambda_s(\sqrt{s}/M_H)$ is twice the expansion parameter $\lambda_s(1)$. For $M_H = 200$ GeV we reach this limit if $\sqrt{s} \approx 4 \times 10^6$ GeV. However, choosing $M_H = 500$ GeV we enter the nonperturbative region for $\sqrt{s} \approx 2500$ GeV. This is already within the \sqrt{s} region considered previously, and the next-to-leading logarithms will be important — if perturbation theory doesn't fail at all.

OMS amplitudes: Introduction of the running coupling $\lambda_s(\sqrt{s}/M_H)$ into the transition amplitude \mathcal{M} results in a resummation of $\ln(s/M_H^2)$ terms. The one-loop running coupling, $\lambda_s^{(1)}$, resums terms of $\mathcal{O}(\lambda^{n+1} \ln^n(s/M_H^2))$, the leading logarithms (LL). The LL amplitude is hence obtained by the tree-level result of the amplitude in connection with the one-loop running coupling. The LL amplitude therefore depends on s — in contrast to the naive

³For $M_H = 500$ GeV the one-loop Landau pole of the one-loop coupling is located at $\sqrt{s} \approx 12\text{TeV}$.

tree-level amplitude using λ_{OMS} . The next-to-leading-log (NLL) amplitude corresponds to the one-loop amplitude using a two-loop running coupling. This resums contributions $\mathcal{O}(\lambda^{n+2} \ln^n(s/M_H^2))$ to the amplitude to all orders. Finally, the next-to-next-to-leading-log amplitude (NNLL) is obtained by including one more loop in both the amplitude and the running coupling. To clarify this, we give the RG relations between coefficients occurring in the amplitudes and the coefficients of the beta function in Appendix A, using as an example the process $W_L W_L \rightarrow Z_L Z_L$.

Using the running coupling, there is always the question how the scale μ is to be chosen. To resum the complete logarithmic dependence of the amplitude (or cross section), one chooses $\mu = \sqrt{s}$ (and $\mu_0 = M_H$ as stated earlier). Of course, there is the possibility to choose μ different from \sqrt{s} . Presently, there is no physical motivation which would suggest not to resum the complete logarithmic dependence. Therefore we take $\mu = \sqrt{s}$ throughout this paper. For a discussion on the dependence of the cross section on the choice of μ we refer to [10].

Using the perturbative OMS amplitude of the previous section, Eq. (4.9), we obtain the NNLL amplitude of the channel $W_L^+ W_L^- \rightarrow Z_L Z_L$ in which the complete logarithmic dependence has been resummed ($\mu = \sqrt{s}$):

$$\begin{aligned}
W_L^+ W_L^- \rightarrow Z_L Z_L : \quad & \text{OMS with running coupling} \\
\mathbf{a}_{j=0}^{\text{NNLL}}(s) = & \frac{N_i N_f}{32\pi} \left(\frac{4|\vec{p}_i||\vec{p}_f|}{s} \right)^{1/2} \Gamma_w^4 \left(-4 \lambda_s^{(3)}(\sqrt{s}/M_H) \right) \left[1 \right. \\
& - \left(21.32 + 25.13 i \right) \frac{\lambda_s^{(3)}(\sqrt{s}/M_H)}{16\pi^2} \\
& \left. + \left(684.4 + 1097.0 i \right) \frac{\left[\lambda_s^{(3)}(\sqrt{s}/M_H) \right]^2}{(16\pi^2)^2} \right]. \tag{5.12}
\end{aligned}$$

The results for the other relevant $2 \rightarrow 2$ scattering amplitudes of the Higgs sector are given in Appendix B. Their relative sizes are very similar to the $W_L^+ W_L^- \rightarrow Z_L Z_L$ channel discussed.

In Eq. (5.12) the factor Γ_w depends on the anomalous dimension of the Goldstone fields and resums a small residual dependence on $\ln(s/M_H^2)$ at two loops. Using Eq. (5.4), Γ_w is given by [7,22]

$$\Gamma_w = \exp \left(\frac{-\gamma_{w,0}}{\beta_0} \frac{\lambda_s(\sqrt{s}/M_H) - \lambda_s(1)}{16\pi^2} \right) \approx \left(\frac{\sqrt{s}}{M_H} \right)^{\frac{-\gamma_{w,0}\lambda_s^2}{16\pi^2}}. \tag{5.13}$$

For channels involving external Higgs fields, we also need

$$\Gamma_H = \exp \left(\frac{-\gamma_{H,0}}{\beta_0} \frac{\lambda_s(\sqrt{s}/M_H) - \lambda_s(1)}{16\pi^2} \right) \approx \left(\frac{\sqrt{s}}{M_H} \right)^{\frac{-\gamma_{H,0}\lambda_s^2}{16\pi^2}}. \tag{5.14}$$

Because of the smallness of the anomalous dimensions, Eqs. (5.7), (5.8), these factors are very close to unity: If $M_H \leq 500$ GeV and $M_H \leq \sqrt{s} \leq 4000$ GeV then $0.980 < \Gamma_H < 1$ and $1 < \Gamma_w < 1.006$, where the largest difference from unity corresponds to the largest values of M_H and \sqrt{s} .

The NLL amplitude is obtained from Eq. (5.12) by dropping the two-loop correction terms and using $\lambda_s^{(2)}$. In addition, the factors Γ_w and Γ_H are unity since the anomalous dimensions vanish at one loop.

Looking at Eq. (5.12), it is interesting to note that the magnitude of the ratio of one-loop to tree-level coefficient is about $20/(16\pi^2) \approx 0.13$, and the two-loop to one-loop ratio is roughly $40/(16\pi^2) \approx 0.25$ in magnitude. Since the running coupling is larger than one for a large range of Higgs masses (see Fig. 3) the perturbative character of the series is already doubtful.

It is clear that the LL result can only provide for a first — possibly excellent — estimate of the amplitude. In Fig. 4 we discuss the importance of the NLL and NNLL corrections for the high-energy amplitudes. We show the real part of the $j = 0$ partial-wave projected amplitude of the channel $W_L^+ W_L^- \rightarrow Z_L Z_L$ in various approximations: LL, NLL, and NNLL. The left plot shows the result for $M_H = 300$ GeV. At $\sqrt{s} = 1000$ GeV, the magnitude of the LL result is reduced by about 10% when going from LL to NLL approximation. At $\sqrt{s} = 4000$ GeV, the reduction amounts to 20%. The additional correction from the NNLL calculation is at most a few percent for the whole range of \sqrt{s} considered. The perturbative amplitude shows a nice convergence. The right plot of Fig. 4 shows the same quantity taking $M_H = 450$ GeV. The larger Higgs mass causes a larger running coupling, leading to a larger amplitude and larger corrections. At $\sqrt{s} = 1000$ GeV, the LL result is reduced by 30% when including the NLL corrections, and at $\sqrt{s} = 4000$ GeV the NLL corrections are even 50%. The NNLL are important for the whole range of \sqrt{s} shown and also need to be included when discussing cross sections.

OMS cross sections: We now investigate the impact of our previous findings when calculating physical observables, i.e., cross sections.⁴ We write the transition amplitude \mathcal{M}^{if} of the scattering process as

$$\mathcal{M}^{if} = \mathcal{M}^{(0)} \lambda_s + \mathcal{M}^{(1)} \lambda_s^2 + \mathcal{M}^{(2)} \lambda_s^3 + \dots, \quad (5.15)$$

where $\mathcal{M}^{(0)}$ is real. The two-loop perturbative cross section in the cm system is

$$\begin{aligned} \sigma_{if} = \frac{N_i^2 N_f^2}{32\pi s} \frac{|\vec{p}_f|}{|\vec{p}_i|} \Gamma_i^4 \Gamma_f^4 \int_{-1}^1 d\cos\theta \Big[(\mathcal{M}^{(0)})^2 \lambda_s^2 + 2\mathcal{M}^{(0)} \text{Re} \mathcal{M}^{(1)} \lambda_s^3 \\ + \left(2\mathcal{M}^{(0)} \text{Re} \mathcal{M}^{(2)} + (\text{Re} \mathcal{M}^{(1)})^2 + (\text{Im} \mathcal{M}^{(1)})^2 \right) \lambda_s^4 + \mathcal{O}(\lambda_s^5) \Big]. \end{aligned} \quad (5.16)$$

The indices i, f label the four possible neutral two-body states for the $2 \rightarrow 2$ process $i \rightarrow f$. We use the resummed form of the transition amplitude, i.e., the logarithms are almost completely absorbed in the running coupling λ_s , and a small two-loop logarithmic dependence is resummed using Γ_i and Γ_f . To have a perturbatively consistent two-loop cross section, we drop terms of $\mathcal{O}([\lambda_s]^5)$ since they get additional contributions from diagrams involving three loops. The one-loop cross section is obtained by dropping all $\mathcal{O}([\lambda_s]^4)$ terms and setting $\Gamma_i = \Gamma_f = 1$.

⁴Re a_0 is not a measurable quantity. Only $|a_0|^2$ is measurable, and it is closely related to the cross section discussed here.

We now discuss the total cross section of the channel $W_L^+ W_L^- \rightarrow Z_L Z_L$. Using the analytical two-loop results of Appendix A, the perturbative result of the high-energy resummed cross section is

$$\sigma_{\text{OMS}}^{\text{NNLL}} = \frac{N_i^2 N_f^2 |\vec{p}_f|}{4\pi s} \frac{|\vec{p}_i|}{|\vec{p}_i|} \Gamma_w^8 [\lambda_s^{(3)}]^2 \left[1 - 42.65 \frac{\lambda_s^{(3)}}{16\pi^2} + 2457.9 \frac{[\lambda_s^{(3)}]^2}{(16\pi^2)^2} + \mathcal{O}([\lambda_s^{(3)}]^3) \right]. \quad (5.17)$$

The magnitude of the ratio of one-loop to tree-level coefficient is about $40/(16\pi^2) \approx 0.25$, and the ratio of two- to one-loop coefficient is about $60/(16\pi^2) \approx 0.4$: The convergence of the cross section is apparently worse than the convergence of the amplitudes, Eq. (5.12). The reason is the fact that the one-loop correction of the cross section is enhanced by a factor two relative to the one-loop correction of the real part of the amplitude. Hence the NLL corrections should always be included in the cross section. At two loops, the squares of the one-loop real and imaginary part also contribute to the two-loop correction, adding in magnitude to other two-loop contributions. Depending on the value of the running coupling, the NNLL correction may be very large.

In Fig. 5 we show the cross section for the process $W_L^+ W_L^- \rightarrow Z_L Z_L$ as a function of the cms-energy, choosing the Higgs mass to be $M_H = 300$ GeV (left plot) and $M_H = 450$ GeV (right plot). To discuss the impact of resumming logarithmic terms at various levels, we show the one-loop cross section using both one-loop and two-loop running coupling, the latter yielding the properly resummed NLL cross section. The first combination does not give a full resummation of NLL terms, i.e. $\mathcal{O}(\lambda_s^{n+2} \ln^n(s/M_H^2))$. The two-loop cross section is also given at two different levels of resummation: In connection with the two-loop running coupling not all NNLL terms are resummed, whereas the use of the three-loop running coupling gives the completely resummed NNLL cross section.

For $M_H = 300$ GeV (left plot), the four different results are very similar, with the one-loop results differing less than 20 percent from the two-loop results for the whole range of energies considered. More importantly, at a given order it is not very important whether the full set of higher-order logarithmic terms is resummed or not. In particular, the two different two-loop approximations yield almost identical results.

For $M_H = 450$ GeV (right plot), the situation is very different. The two-loop results are much larger than the one-loop results. At $\sqrt{s} = 1500$ GeV, the two-loop cross section is about a factor two larger than the one-loop cross section. The difference between the two orders of calculation is even larger for higher energies. It is interesting that the level of resummation of higher-order logarithmic terms is still much less important than the order of the calculation. It is the non-logarithmic terms which are the cause of the large corrections, and their importance increases for increasing Higgs coupling, that is, increasing \sqrt{s} and/or M_H . For large values of \sqrt{s} and/or M_H perturbation breaks down. This is documented most strikingly by the one-loop perturbative cross section which can become negative since the one-loop correction to the perturbative cross section has the opposite sign of the tree-level term; see Eq. (5.17).⁵ For $M_H = 450$ GeV and using the one-loop running coupling, the

⁵The perturbative cross section is not positive definite since higher-order terms are dropped when squaring the amplitude.

one-loop cross section is negative for $\sqrt{s} \gtrsim 3870$ GeV, a clear signal for the breakdown of perturbation theory. Looking at Eq. (5.17) we find that the one-loop perturbative cross section becomes negative if $\lambda_s \geq 16\pi^2/42.65 \approx 3.7$, independent of a particular choice of M_H and \sqrt{s} . For $M_H = 300$ (450) GeV, the one-loop running coupling $\lambda_s^{(1)}$ is larger than 3.7 if $\sqrt{s} \gtrsim 3.5 \times 10^5$ (3870) GeV. Using the two-loop running coupling $\lambda_s^{(2)}$, the one-loop NLL cross section can also be negative. Requiring $\lambda_s^{(2)} \gtrsim 3.7$ the one-loop NLL cross section becomes negative for $\sqrt{s} \gtrsim 7800$ GeV if $M_H = 450$.

Our findings based on the above cross sections indicate that it is *impossible* to make a satisfactory perturbative prediction for the high-energy cross section for $W_L^+ W_L^- \rightarrow Z_L Z_L$ from perturbation theory if $\lambda_s \approx 3.7$. Examining the cross sections of the other $2 \rightarrow 2$ channels of our scattering matrix, we find critical values in the range of $\lambda_s = 3.1$ to 4.1, depending on the size of the one-loop coefficient. To obtain reliable perturbative cross sections, the minimal requirement is

$$\lambda_s < 3.1. \quad (5.18)$$

Keeping in mind that the non-running coupling $\lambda_{\text{OMS}} \approx 3$ for $M_H = 600$ GeV and that $\lambda_s > \lambda_{\text{OMS}}$ for $\sqrt{s} > M_H$, the requirement $\lambda_s < 3.1$ is already a strong constraint on a perturbative Higgs mass if we want to predict high-energy cross sections for $\sqrt{s} \gtrsim 2M_H$. To find out how much smaller than 3.1 the running coupling has to be, we consider the case $M_H = 450$ GeV and $\sqrt{s} \gtrsim 3M_H$: Then the running coupling $\lambda_s^{(n)}$ is always larger than 2.2. This choice refers to the right plot of Fig. 5 with $\sqrt{s} \geq 1350$ GeV. In this region, the two-loop cross section is more than twice the size of the one-loop cross section. The perturbativity of the result is therefore questionable for values of λ_s as low as 2.2. Vice versa, requiring that the NLL cross section and the NNLL differ by less than a factor two we find an upper bound on a perturbative running coupling of

$$\lambda_s \leq 2.2. \quad (5.19)$$

The bounds from Eqs. (5.18) and (5.19) give limits on the maximal energy up to which perturbative calculations of $2 \rightarrow 2$ in the Higgs sector are possible. These bounds are shown in Fig. 6 where we consider values of \sqrt{s} larger than 4 TeV.

To illustrate the importance of our findings for future phenomenological applications, we compare the RG results of the high-energy cross section with the non-resummed one-loop result which contains both λ and λv contributions, i.e., the exact EQT result at one loop. In the left plot of Fig. 7 we show the cross section of $W_L^+ W_L^- \rightarrow Z_L Z_L$ for $M_H = 450$ GeV. For $\sqrt{s} < 2M_H$ the cross section is dominated by the resonant contribution from s-channel Higgs exchange. For larger values of \sqrt{s} , the high-energy contribution, solely connected to the quartic coupling, dominates the cross section; also recall Table I. The actual size of the cross section, however, has large uncertainties due to the bad convergence of the RG improved cross section.

A similar behaviour can be found for all other $2 \rightarrow 2$ cross sections involving W_L^\pm , Z_L , and H . Phenomenologically, the process $W_L^+ W_L^- \rightarrow W_L^+ W_L^-$ is the most important one for LHC and NLC physics. We show its cross section in the right plot of Fig. 7, also taking $M_H = 450$ GeV. This channel has a significantly larger cross section than the previous one. The relative size of the radiative corrections is slightly larger than the one of the process $W_L^+ W_L^- \rightarrow Z_L Z_L$. This is due to the fact that the one-loop real part of amplitude is larger in

the $W_L^+ W_L^- \rightarrow W_L^+ W_L^-$ channel, see Eqs. (B1) and (B3). We find that the actual size of the cross section has again large uncertainties due to the bad convergence of the RG improved cross section if M_H is larger than $O(450 \text{ GeV})$ and $\sqrt{s} \gtrsim 2M_H$. We conclude that using perturbative methods a future experimental extraction of the quartic coupling from such cross sections is very unreliable for Higgs masses of $O(450 \text{ GeV})$.

The one-loop cross section of $W_L^+ W_L^- \rightarrow W_L^+ W_L^-$ was already presented in Fig. 8 of [11] for $M_H = 500 \text{ GeV}$ and \sqrt{s} in the range of 250 to 3000 GeV. Though the authors state the importance of resumming large logarithms using a running coupling, their cross sections are plotted using a non-running coupling $\lambda = \lambda_{\text{OMS}}$. Our results of Fig. 7 show that the use of the running coupling is very important for \sqrt{s} in the TeV range, and that $M_H = 500 \text{ GeV}$ is already too large to yield a reliable perturbative answer for $\sqrt{s} \geq 1.5 \text{ TeV}$. For $1000 \lesssim \sqrt{s} < 1.5 \text{ TeV}$, a NNLL perturbative answer may give a reasonable estimate of the high-energy contribution to the cross section.

B. RGE in $\overline{\text{MS}}$ FORMULATION

Since the perturbative behaviour of the OMS high-energy amplitudes and cross sections is not satisfactory for $M_H \gtrsim 450 \text{ GeV}$, we also investigate the RGE in the $\overline{\text{MS}}$ scheme, hoping to find improved convergence. The relevant renormalization group equation is given in Eq. (5.2). Introducing the three-loop $\overline{\text{MS}}$ running coupling, $\overline{\lambda}_s$, we can resum all $\ln(s/\mu^2)$ terms to NNLL order. The two-loop $\ln(s/M_H^2)$ term of Eq. (4.11) is connected to the field anomalous dimensions.

The $\overline{\text{MS}}$ three-loop running coupling differs from the OMS one through a different value for $\lambda_s(1)$, the value of the running coupling at the scale $\mu = \mu_0$, and a different value of the scheme dependent three-loop coefficient $\beta_2^{\overline{\text{MS}}} = 12\,022.69 \dots$ [24,23,10]. In agreement with our approach in the OMS scheme, we choose $\mu_0 = M_H$.⁶ This defines $\lambda_s(1)$ as the value of the $\overline{\text{MS}}$ coupling at scale M_H , and it can be calculated using Eq. (3.6). The resulting $\overline{\text{MS}}$ value is denoted by $\overline{\lambda}_s(1)$, and it is larger than the corresponding value in the OMS scheme. Consequently, the $\overline{\text{MS}}$ running coupling is also larger than the OMS running coupling. Since the coefficients of the $\overline{\text{MS}}$ amplitudes are already in magnitude larger than the OMS coefficients, recall Eq. (4.11), the convergence of the $\overline{\text{MS}}$ amplitudes is worse than the convergence of the OMS results. To show this explicitly, we give the $\overline{\text{MS}}$ result of the two-loop high-energy cross section of $W_L^+ W_L^- \rightarrow Z_L Z_L$:

$$\sigma_{\overline{\text{MS}}}^{\text{NNLL}} = \frac{N_i^2 N_f^2 |\vec{p}_f|}{4\pi s |\vec{p}_i|} \Gamma_w^8 [\overline{\lambda}_s^{(3)}]^2 \left[1 - 60 \frac{\overline{\lambda}_s^{(3)}}{16\pi^2} + 3370.7 \frac{[\overline{\lambda}_s^{(3)}]^2}{(16\pi^2)^2} + O([\overline{\lambda}_s^{(3)}]^3) \right]. \quad (5.20)$$

This result is to be compared with the OMS cross section, Eq. (5.17): The $\overline{\text{MS}}$ corrections are significantly larger than the OMS corrections.

Analogous to the OMS case, the one-loop perturbative cross section can become negative if $\overline{\lambda}_s$ is too large. In the $\overline{\text{MS}}$ scheme, this happens for a running coupling of $\overline{\lambda}_s \geq 16\pi^2/60 \approx$

⁶Different choices of μ_0 are discussed in [9,10].

2.6. Taking $M_H = 450$ GeV, the one-loop $\overline{\text{MS}}$ running coupling reaches this critical value for $\sqrt{s} = 1300$ GeV, and the two-loop $\overline{\text{MS}}$ running coupling is equal to 2.6 for $\sqrt{s} = 1500$ GeV, values much lower than the OMS results of 3870 and 7800 GeV, respectively. This indicates a large scheme dependence of the perturbative results, another sign of the breakdown of perturbation theory.

We conclude that our OMS result – taking $M_H = \text{O}(450 \text{ GeV})$ to be the upper limit for perturbative high-energy ($\sqrt{s} \gtrsim 2M_H$) calculations in the Higgs sector – is strengthened by the $\overline{\text{MS}}$ results. To achieve the best apparent convergence of the perturbative results, the OMS scheme should be employed.

Our constraints on the running coupling from a two-loop analysis can be compared with the results obtained from a two-loop analysis of unitarity constraints which was carried out in [25]. In that paper the OMS scheme is used, and the running coupling is defined using $\mu_0 \approx 0.7M_H$ as suggested by [9]. This different choice of μ_0 corresponds to a resummation of constant terms, resulting in larger magnitudes of the subleading coefficients of the perturbative amplitudes compared to our OMS result with $\mu_0 = M_H$. In fact, the bounds received in [25] are similar to the $\overline{\text{MS}}$ constraints found here, i.e., somewhat more stringent than the OMS results of the previous subsection.

VI. SUMMARY

The Higgs quartic coupling dominates the cross sections of elastic $2 \rightarrow 2$ processes involving longitudinally polarized gauge bosons and the Higgs boson for $\sqrt{s} \gtrsim 1.5 - 2M_H$. Using perturbative amplitudes up to two loops and considering cms energies of up to 4 TeV, we find the cross sections to have large uncertainties if $\sqrt{s} \gtrsim 2M_H$ and $M_H \gtrsim 450$ GeV. This is due to a unsatisfactory convergence of the perturbative series in the OMS scheme. The breakdown of perturbation theory is due to large logarithmic terms (which lead to a large running coupling) as well as large non-logarithmic contributions to the perturbative cross section. One-loop and two-loop high-energy cross sections differ factors of two or more if M_H is $\text{O}(450 \text{ GeV})$. Simultaneously, the cross section exhibits a large renormalization scheme dependence as seen in the comparison of OMS and $\overline{\text{MS}}$ results, with the OMS scheme giving a better convergence of the perturbative series. The large uncertainties in the perturbative cross sections will inhibit the analysis of the quartic Higgs coupling in the case of a heavy Higgs, $M_H \gtrsim 450$ GeV, decreasing the experimental sensitivity to physics beyond the Standard Model significantly.

If $M_H \lesssim 350$ GeV, the apparent convergence of the perturbation series is satisfactory, still assuming $\sqrt{s} \lesssim 4$ TeV. However, for energies $\sqrt{s} > 2M_H$ it is essential to resum the leading logarithmic energy dependence to all orders using the running coupling. NLL terms are subdominant, and the Standard Model cross sections for longitudinal gauge boson scattering can be predicted with errors of less than 10% if the NNLL approximation is used, sufficient for LHC and future NLC experiments.

VII. ACKNOWLEDGMENTS

The author would like to thank L. Durand and U. Nierste for many useful discussions. Further stimulation and information was provided through discussions with A. Buras, R. Hempfling, B. Kniehl, M. Lindner, and A. Sirlin. This work was partially supported by the Deutsche Forschungsgemeinschaft (DFG) under contract number Li519/2-1.

APPENDIX A: ANGULAR DEPENDENT RESULT OF $W_L^+ W_L^- \rightarrow Z_L Z_L$

We write the high-energy transition amplitudes of the process $W_L^+ W_L^- \rightarrow Z_L Z_L$ in the general form

$$\begin{aligned} \mathcal{M} = & c_{10} \lambda + \left[c_{21} \ln(s/\mu^2) + c_{20} + d_{20} \left[\ln(-t/s) + \ln(-u/s) \right] \right] \frac{\lambda^2}{16\pi^2} \\ & + \left[c_{32} \ln^2(s/\mu^2) + c_{31} \ln(s/\mu^2) + c'_{31} \ln(s/M_H^2) + c_{30} \right. \\ & + \left[d_{31} \ln(s/\mu^2) + d_{30} \right] \left[\ln(-t/s) + \ln(-u/s) \right] \\ & \left. + e_{30} \left[\ln^2(-t/s) + \ln^2(-u/s) \right] \right] \frac{\lambda^3}{(16\pi^2)^2}, \end{aligned} \quad (\text{A1})$$

a form which is adequate for all $t \leftrightarrow u$ symmetric channels. No renormalization scheme has been specified. In the OMS-renormalization scheme, the scale μ is defined as $\mu = M_H$.

The quantities s , $-t$, and $-u$ are real and positive in the physical region. The terms $\ln(-t/s)$ and $\ln(-u/s)$ are a function of only the scattering angle. In the center-of-mass system we have $-t/s = (1 + \cos \theta_{cm})/2$, $-u/s = (1 - \cos \theta_{cm})/2$.

The coefficients c_{nm} correspond to terms independent of the scattering angle. Coefficients d_{nm} and e_{nm} refer to terms containing an angular dependence as $\ln(1 \pm \cos \theta)$ and $\ln^2(1 \pm \cos \theta)$, respectively. The index n refers to the order in perturbation theory, λ^n . The index m indicates the power in $\ln(s)$. In the OMS scheme, the coefficients can be calculated using the results of [7]. The $\overline{\text{MS}}$ coefficients are then derived as outlined in the text. To indicate the scheme dependence of the different coefficients as well as the connection of certain coefficients to the beta function, we give the explicit analytical result in the case of $W_L^+ W_L^- \rightarrow Z_L Z_L$. Coefficients with a bar indicate $\overline{\text{MS}}$ quantities, others are OMS quantities. Recall that $\overline{\beta}_0 = \beta_0$ and $\overline{\beta}_1 = \beta_1$.

Tree level :

$$c_{10} = \overline{c}_{10} = -2. \quad (\text{A2})$$

One loop :

$$c_{21} = \overline{c}_{21} = \frac{\beta_0}{2} c_{10} = -24, \quad (\text{A3})$$

$$c_{20} = 2 + 6\pi\sqrt{3} + 16\pi i \approx 34.648 + 50.265 i, \quad (\text{A4})$$

$$\overline{c}_{20} = 52 + 16\pi i \quad (\text{A5})$$

$$d_{20} = \overline{d}_{20} = -4. \quad (\text{A6})$$

Two loops :

$$c_{32} = \bar{c}_{32} = \left(\frac{\beta_0}{2}\right)^2 c_{10} = -288, \quad (\text{A7})$$

$$c_{31} = \frac{\beta_1}{2} c_{10} + \beta_0 c_{20} = 360 + 144\pi\sqrt{3} + 384\pi i \approx 1143.561 + 1206.372 i, \quad (\text{A8})$$

$$\bar{c}_{31} = \frac{\beta_1}{2} \bar{c}_{10} + \beta_0 \bar{c}_{20} = 1560 + 384\pi i, \quad (\text{A9})$$

$$c'_{31} = \bar{c}'_{31} = -24, \quad (\text{A10})$$

$$d_{31} = \bar{d}_{31} = \beta_0 d_{20} = -96, \quad (\text{A11})$$

$$c_{30} = -74 - 224\zeta(2) + 180\zeta(3) - 384\mathbf{Cl}\sqrt{3} + 138\pi\sqrt{3} - 96\pi\mathbf{Cl} - 324K_5 \\ - (176\pi + 96\pi^2\sqrt{3})i \approx -755.583 - 2194.007 i, \quad (\text{A12})$$

$$\bar{c}_{30} = -2524 + 824\zeta(2) + 48\mathbf{Cl}\sqrt{3} - 976\pi i \approx -1084.194 - 3066.194, \quad (\text{A13})$$

$$d_{30} = 80 + 24\pi\sqrt{3} \approx 210.594, \quad (\text{A14})$$

$$\bar{d}_{30} = 280, \quad (\text{A15})$$

$$e_{30} = \bar{e}_{30} = -48, \quad (\text{A16})$$

where the constants $\zeta(2)$, $\zeta(3)$, \mathbf{Cl} , and K_5 are defined following Eq. (3.6) in the text.

APPENDIX B: PARTIAL-WAVE PROJECTED AMPLITUDES

Here we give the OMS high-energy results for the $j = 0$ partial-wave projected amplitudes for all $2 \rightarrow 2$ channels considered. They are derived using the results of [7]. The running coupling is understood to be the two-loop running coupling, $\lambda_s \equiv \lambda_s^{(2)}$, defined in Eqs. (5.10), (5.11). If the three-loop running coupling becomes available, it can be used without a change in the coefficients presented here, leading to a complete resummation of all NNLL terms. The overall factor $(4|\vec{p}_i||\vec{p}_f|/s)^{1/2}$ is taken to be unity (high-energy limit).

$W_L^+ W_L^- \rightarrow W_L^+ W_L^- :$

$$\mathbf{a}_0(s) = \frac{-8\lambda_s^{(2)}\Gamma_w^4}{32\pi} \left[1 - \left(24.32 + 15.71 i \right) \frac{\lambda_s^{(2)}}{16\pi^2} + \left(1233.6 + 713.9 i \right) \left[\frac{\lambda_s^{(2)}}{16\pi^2} \right]^2 \right]. \quad (\text{B1})$$

$Z_L Z_L \rightarrow Z_L Z_L :$

$$\mathbf{a}_0(s) = \frac{-12\lambda_s^{(2)}\Gamma_w^4}{64\pi} \left[1 - \left(25.32 + 12.57 i \right) \frac{\lambda_s^{(2)}}{16\pi^2} + \left(1416.7 + 586.2 i \right) \left[\frac{\lambda_s^{(2)}}{16\pi^2} \right]^2 \right]. \quad (\text{B2})$$

$W_L^+ W_L^- \rightarrow Z_L Z_L :$

$$\mathbf{a}_0(s) = \frac{-4\lambda_s^{(2)}\Gamma_w^4}{32\pi\sqrt{2}} \left[1 - \left(21.32 + 25.13 i \right) \frac{\lambda_s^{(2)}}{16\pi^2} + \left(684.3 + 1097.0 i \right) \left[\frac{\lambda_s^{(2)}}{16\pi^2} \right]^2 \right]. \quad (\text{B3})$$

$HH \rightarrow W_L^+ W_L^- :$

$$\mathbf{a}_0(s) = \frac{-4 \lambda_s^{(2)} \Gamma_w^2 \Gamma_H^2}{32\pi\sqrt{2}} \left[1 - \left(19.21 + 25.13 i \right) \frac{\lambda_s^{(2)}}{16\pi^2} + \left(606.5 + 1043.7 i \right) \left[\frac{\lambda_s^{(2)}}{16\pi^2} \right]^2 \right]. \quad (\text{B4})$$

$HH \rightarrow Z_L Z_L :$

$$\mathbf{a}_0(s) = \frac{-4 \lambda_s^{(2)} \Gamma_w^2 \Gamma_H^2}{64\pi} \left[1 - \left(19.21 + 25.13 i \right) \frac{\lambda_s^{(2)}}{16\pi^2} + \left(606.5 + 1043.7 i \right) \left[\frac{\lambda_s^{(2)}}{16\pi^2} \right]^2 \right]. \quad (\text{B5})$$

$HH \rightarrow HH :$

$$\mathbf{a}_0(s) = \frac{-12 \lambda_s^{(2)} \Gamma_H^4}{64\pi} \left[1 - \left(21.09 + 12.57 i \right) \frac{\lambda_s^{(2)}}{16\pi^2} + \left(1248.6 + 532.9 i \right) \left[\frac{\lambda_s^{(2)}}{16\pi^2} \right]^2 \right]. \quad (\text{B6})$$

$HZ_L \rightarrow HZ_L :$

$$\mathbf{a}_0(s) = \frac{-4 \lambda_s^{(2)} \Gamma_w^2 \Gamma_H^2}{32\pi} \left[1 - \left(25.21 + 6.28 i \right) \frac{\lambda_s^{(2)}}{16\pi^2} + \left(1692.3 + 317.5 i \right) \left[\frac{\lambda_s^{(2)}}{16\pi^2} \right]^2 \right]. \quad (\text{B7})$$

The explicit $\ln(s)$ dependence up to two loops can be obtained by expanding $\lambda_s^{(2)}$, Γ_w , and Γ_H in power of $\lambda_s(1) \equiv \lambda_{\text{OMS}}$, dropping terms of $\mathcal{O}(\lambda_{\text{OMS}}^4)$. The constant terms given above will not receive any corrections since our definition of the running coupling, Eq. (5.10), does not involve any resummation of constant terms.

The $j = 0$ partial-wave projected amplitude can be used to calculate the total cross section in very good approximation. Since the tree-level high-energy amplitude is independent of the scattering angle, only the $j = 0$ partial wave is non-zero. Including higher order corrections, the matrix elements depend on the scattering angle, but with rather small coefficients. The $j = 0$ partial-wave projected cross section remains dominant and is an excellent approximation of the total two-loop cross section:

$$\sigma \approx \frac{4\pi}{|\vec{p}_i|^2} |\mathbf{a}_{j=0}|^2, \quad (\text{B8})$$

where $|\mathbf{a}_{j=0}|^2$ is understood to be expanded in powers of λ_s , dropping terms of $\mathcal{O}([\lambda_s^{(2)}]^5)$. At one loop, neglecting terms of $\mathcal{O}(\lambda_s^4)$, the total cross section is actually *equal* to the $j = 0$ cross section. At two loops, the λ_s^4 coefficients are not identical anymore, but their numerical difference is much less than 1%. The $j = 0$ partial-wave projected cross section of the channel $W_L^+ W_L^- \rightarrow Z_L Z_L$, for example, has a two-loop coefficient of 2455.1, whereas the total cross section, given in Eq. (5.17), has the coefficient 2457.9.

REFERENCES

- [1] P.W. Higgs, Phys. Lett. **122**, 132 (1964), Phys. Rev. Lett. **13**, 508 (1964), Phys. Rev. **145**, 1156 (1966); F. Englert and R. Brout, Phys. Rev. Lett. **13**, 321 (1964); G.S. Guralnik, C.R. Hagen, and T.W.B. Kibble, Phys. Rev. Lett. **13**, 585 (1964); T.W.B. Kibble, Phys. Rev. **155**, 1554 (1967).
- [2] J.M. Cornwall, D.N. Levin, and G. Tiktopoulos, Phys. Rev. D **10**, 1145 (1974); (E) **11**, 972 (1975); C.E. Vayonakis, Lett. Nuovo Cim. **17**, 383 (1976); M.S. Chanowitz and M.K. Gaillard, Nucl. Phys. **B261**, 379 (1985); G.J. Gounaris, R. K  gerler, and H. Neufeld, Phys. Rev. D **34**, 3257 (1986); Y.-P. Yao and C.-P. Yuan, *ibid.* **38**, 2237 (1988).
- [3] B.W. Lee, C. Quigg, and H.B. Thacker, Phys. Rev. Lett. **38**, 883 (1977); Phys. Rev. D **16**, 1519 (1977).
- [4] J. Bagger and C. Schmidt, Phys. Rev. D **41**, 264 (1990); H. Veltman, Phys. Rev. D **41**, 2294 (1990); H.-J. He, Y.-P. Kuang, and X. Li, Phys. Rev. Lett. **69**, 2619 (1992); Phys. Rev. D **49**, 4842 (1994); H.-J. He, Y.-P. Kuang, and C.-P. Yuan, Phys. Rev. D **51**, 6463 (1995).
- [5] J. Goldstone, Nuovo Cim. **19**, (1961) 154; Y. Nambu and G. Jona-Lasinio, Phys. Rev. **122**, 345 (1961), Phys. Rev. **124**, 246 (1961); J. Goldstone, A. Salam, and S. Weinberg, Phys. Rev. **127**, 965 (1962).
- [6] R.S. Lytel, Phys. Rev. D **22**, 505 (1980).
- [7] P.N. Maher, L. Durand, and K. Riesselmann, Phys. Rev. D **48**, 1061 (1993); (E) **52**, 553 (1995).
- [8] A. Ghinculov, Phys. Lett. B **337**, 137 (1994); (E) **346**, 426 (1994); A. Ghinculov and J. van der Bij, Nucl. Phys. **B436**, 30 (1995).
- [9] A. Sirlin and R. Zucchini, Nucl. Phys. **B266**, 389 (1986).
- [10] U. Nierste and K. Riesselmann, Techn. Univ. Munich preprint TUM-HEP-224/95 (November 1995), hep-ph/9511407.
- [11] S. Dawson and S. Willenbrock, Phys. Rev. D **40**, 2880 (1989).
- [12] S.N. Gupta, J.M. Johnson, and W.W. Repko, Phys. Rev. D **48**, 2083 (1993); the expressions for $B_3(s=1)$ and $\text{Im } C_5(s)$ contain typographical errors, and a term was left out when typewriting the result of $\text{Im } C_3(s)$. I thank Dr. Johnson for checking the original results.
- [13] S. Dawson and S. Willenbrock, Phys. Rev. Lett. **62**, 1232 (1989).
- [14] W. Marciano, G. Valencia, and S. Willenbrock, Phys. Rev. D **40**, 1725 (1989).
- [15] L. Durand, J.M. Johnson, and J.L. Lopez, Phys. Rev. Lett. **64**, 1215 (1990); Phys. Rev. D **45**, 3112 (1992).
- [16] The resonance pole of the amplitude can be avoided by including a finite width in the Higgs propagator; see e.g. [11]. For $\sqrt{s} \gtrsim 2M_H$ the effect is not significant. For a recent discussion see M. Seymour, preprint CERN-TH/95-94, hep-ph/9505211.
- [17] J. Collins: *Renormalization*, Chap. 7 (Cambridge University Press, Cambridge, 1984).
- [18] A.I. Bochkarev and R.S. Willey, Phys. Rev. D **51**, 2049 (1995); Eq. (17) of this paper uses incorrect numbers.
- [19] K. Riesselmann, in: Proceedings of the Ringberg Workshop on "Perspectives for electroweak interactions in e^+e^- collisions", Munich, Germany (Feb. 5-8, 1995), ed.: B. Kniehl, (World Scientific, Singapore, 1995), p. 175.

- [20] C.G. Callan, Phys. Rev. D **2**, 1541 (1970); K. Symanzik, Comm. Math. Phys. **18**, 227 (1970).
- [21] G. 't Hooft, Nucl. Phys. **B61**, 455 (1973); S. Weinberg, Phys. Rev. D **8**, 3497 (1973).
- [22] T.-P. Cheng and L.-F. Li: *Gauge theory of elementary particle physics*, Chap. 3 (Clarendon Press, Oxford, 1988).
- [23] M. Lüscher and P. Weisz, Nucl. Phys. **B318**, 705 (1989).
- [24] A.A. Vladimirov, D.I. Kazakov, and O.V. Tarasov, Sov. Phys. JETP **50**, 521 (1979).
- [25] L. Durand, P.N. Maher, and K. Riesselmann, Phys. Rev. D **48**, 1084 (1993).

TABLES

	M_H (GeV)	\sqrt{s} (GeV)	$\Delta(a_{j=0}^{\text{tree}})$	$\Delta(\text{Re } a_{j=0}^{\text{1p}})$	$\Delta(\text{Im } a_{j=0}^{\text{1p}})$	
	200	300	44.4	46.4	39.2	
	200	400 ($2M_H$)	25.0	27.1	6.1	
	200	500	16.0	17.8	-6.5	
	200	600 ($3M_H$)	11.1	12.7	-11.2	
	200	800 ($4M_H$)	6.3	7.4	-12.6	
	200	1000 ($5M_H$)	4.0	4.9	-11.1	
	200	2000	1.0	1.4	-4.7	
	200	3000	0.4	0.7	-2.5	
	200	4000	0.2	0.4	-1.6	
	500	750	44.4	56.2	39.2	
	500	1000 ($2M_H$)	25.0	36.9	6.1	
	500	1250	16.0	26.3	-6.5	
	500	1500 ($3M_H$)	11.1	19.8	-11.2	
	500	2000 ($4M_H$)	6.3	12.4	-12.6	
	500	2500 ($5M_H$)	4.0	8.6	-11.1	
	500	3000	2.8	6.3	-9.3	
	500	4000	1.6	4.0	-6.5	
	800	1200	44.4	71.7	39.2	
	800	1600 ($2M_H$)	25.0	51.2	6.1	
	800	2000	16.0	38.0	-6.5	
	800	2400 ($3M_H$)	11.1	29.1	-11.2	
	800	2500	10.2	27.4	-11.8	
	800	3000	7.1	20.5	-12.7	
	800	3200 ($4M_H$)	6.3	18.5	-12.6	
	800	4000 ($5M_H$)	4.0	12.7	-11.1	

TABLE I. The relative difference between the exact EQT amplitude and the high-energy EQT amplitude, $\Delta(a_{j=0}) = (a_{j=0}^{\text{exact}} - a_{j=0}^{\text{high}})/a_{j=0}^{\text{exact}}$, in percent. The first two columns give the values for the Higgs mass and the cms energy in units of GeV. The third column shows the difference at tree level, the forth and fifth column the one-loop difference separated into real and imaginary part, respectively.

FIGURES

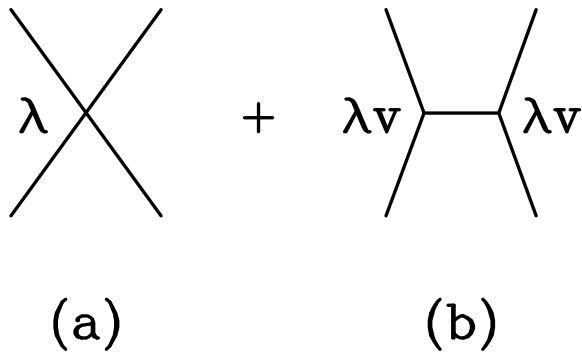


FIG. 1. The two topologies contributing to the $2 \rightarrow 2$ scattering processes at tree level. For $\sqrt{s} \gtrsim 2M_H$ topology (a), the quartic coupling contribution to the amplitude, dominates relative to the trilinear coupling contributions of topology (b).

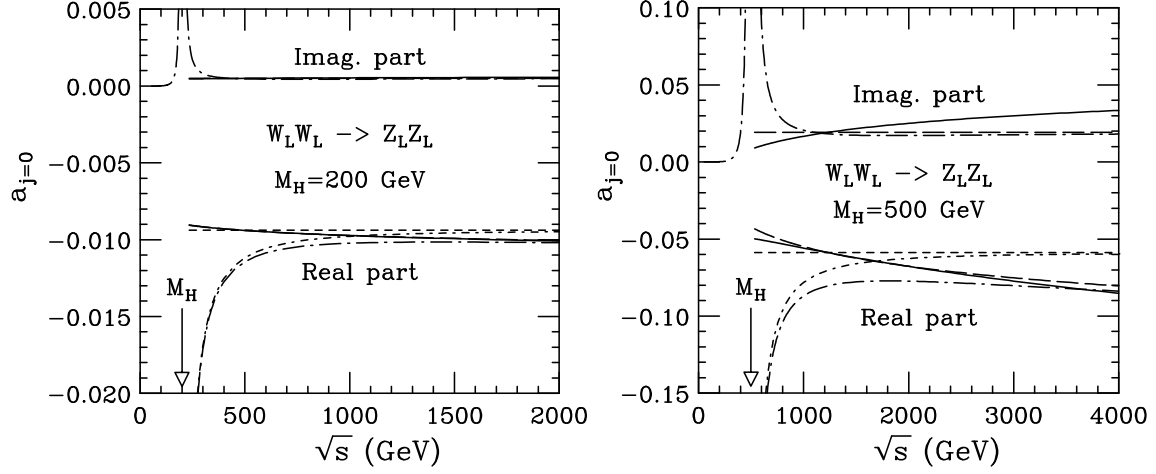


FIG. 2. The $j = 0$ partial-wave projected amplitude for $W_L W_L \rightarrow Z_L Z_L$ in the limit of $M_H \gg M_W$. The Higgs mass is chosen as $M_H = 200$ GeV (left plot) and $M_H = 500$ GeV (right plot). The amplitudes are calculated in exact EQT approximation (dot-dashed curves, results taken from [11,12]) and in high energy EQT approximation (dashed curves, [13–15]). Both tree-level (short dashes) and one-loop (long dashes) results are compared, and we find the high-energy approximation to differ less than 20% for $\sqrt{s} \gtrsim 3M_H$. We also show the two-loop high energy result (solid line). Note the different scales used in the two plots.

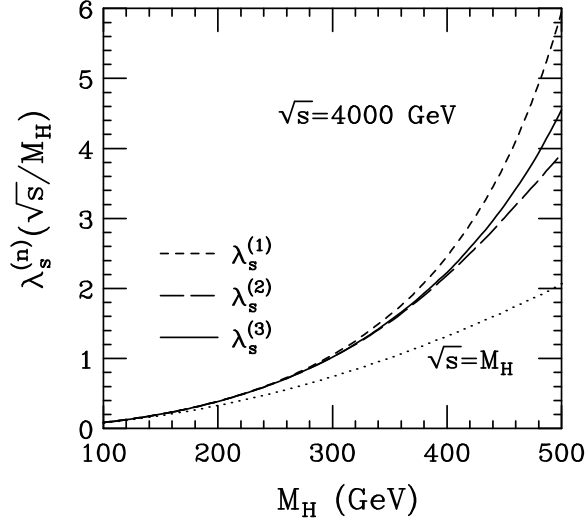


FIG. 3. The OMS running Higgs coupling $\lambda_s^{(n)}(\sqrt{s}/M_H)$ in one-loop ($n=1$), two-loop ($n=2$), and three-loop ($n=3$) approximation. In all cases the running coupling is normalized at $\sqrt{s} = M_H$ such that $\lambda_s^{(n)}(1) = M_H^2/(2v^2)$ (dotted curve). Evolving the coupling to higher energies, the values of $\lambda_s^{(1)}$, $\lambda_s^{(2)}$, $\lambda_s^{(3)}$ are shown for $\sqrt{s} = 4000$ GeV.

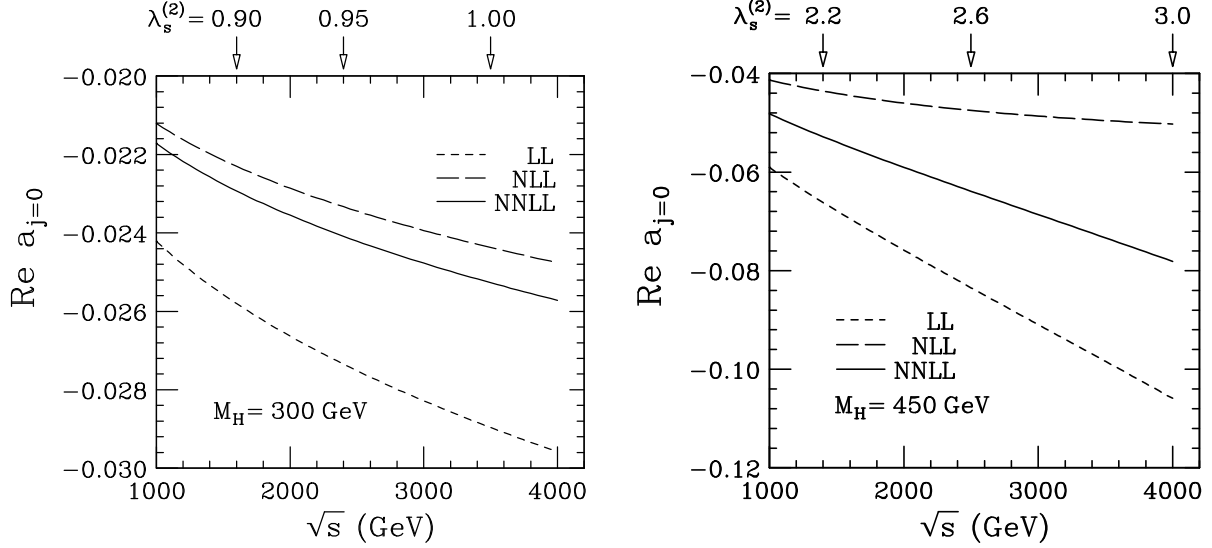


FIG. 4. The real part of the $j = 0$ partial-wave projected amplitude for the process $W_L^+ W_L^- \rightarrow Z_L Z_L$ for $M_H = 300$ GeV (left plot) and $M_H = 450$ GeV (right plot). The amplitudes are calculated using the high-energy approximation. At each order of the perturbative calculation, the complete $\ln(s/M_H^2)$ dependence of the amplitude is resummed using the $(n + 1)$ -loop running coupling $\lambda_s^{(n+1)}$ in connection with the n -loop perturbative amplitude. This yields the LL, NLL, and NNLL results for $n = 1, 2, 3$, respectively. Note the very different scales used in the two plots.

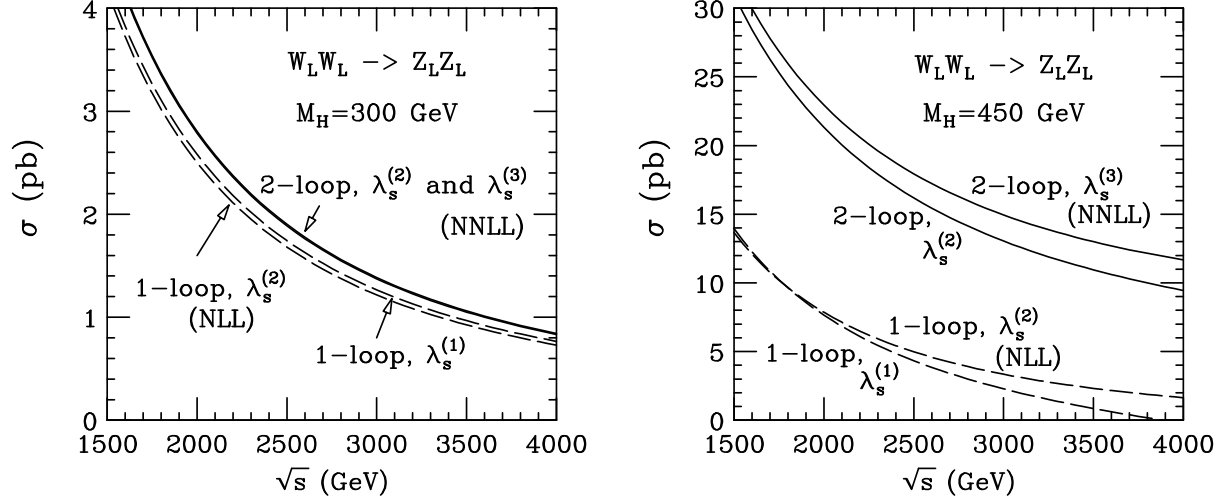


FIG. 5. The cross section of the process $W_L^+ W_L^- \rightarrow Z_L Z_L$ as a function of the cms-scattering energy \sqrt{s} for $M_H = 300$ GeV (left plot) and 450 GeV (right plot). The relative importance of the logarithmic and non-logarithmic contributions is examined at the one-loop and two-loop level. Note that the one-loop perturbative cross section in connection with the one-loop running coupling is negative for $M_H = 450$ GeV and $\sqrt{s} \geq 3870$ GeV.

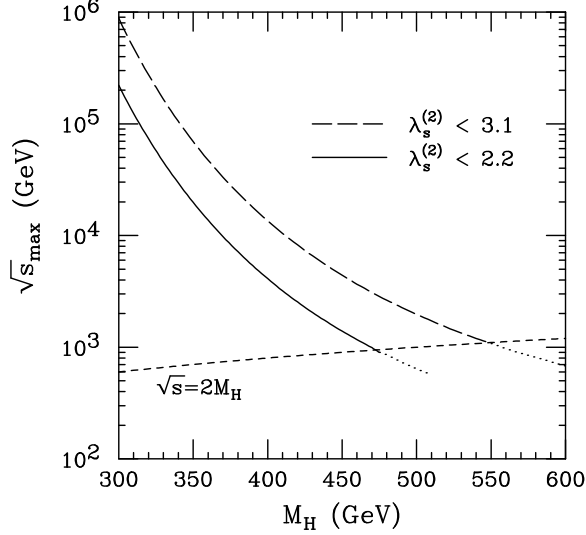


FIG. 6. The maximal cms energy \sqrt{s} up to which a perturbative calculation of $2 \rightarrow 2$ scattering processes in the Higgs sector is possible. The upper bound on \sqrt{s} is derived from $\lambda_s(\sqrt{s}/M_H) < 3.1$ which corresponds to requiring the one-loop RG improved $2 \rightarrow 2$ cross sections to be positive. For larger values of \sqrt{s} (and hence λ_s) perturbation theory completely fails. The stricter bound $\lambda_s < 2.2$ is derived requiring the ratio $\sigma^{\text{NNLL}}/\sigma^{\text{NLL}}$ to be less than two in the OMS scheme, and it leads to a stricter upper bound on \sqrt{s} . Values of $2.2 \lesssim \lambda_s < 3.1$ lead to very unreliable perturbative cross sections. The bounds on \sqrt{s} are calculated using the two-loop running coupling. For the high-energy bounds to be applicable, we need $\sqrt{s} > 2M_H$.

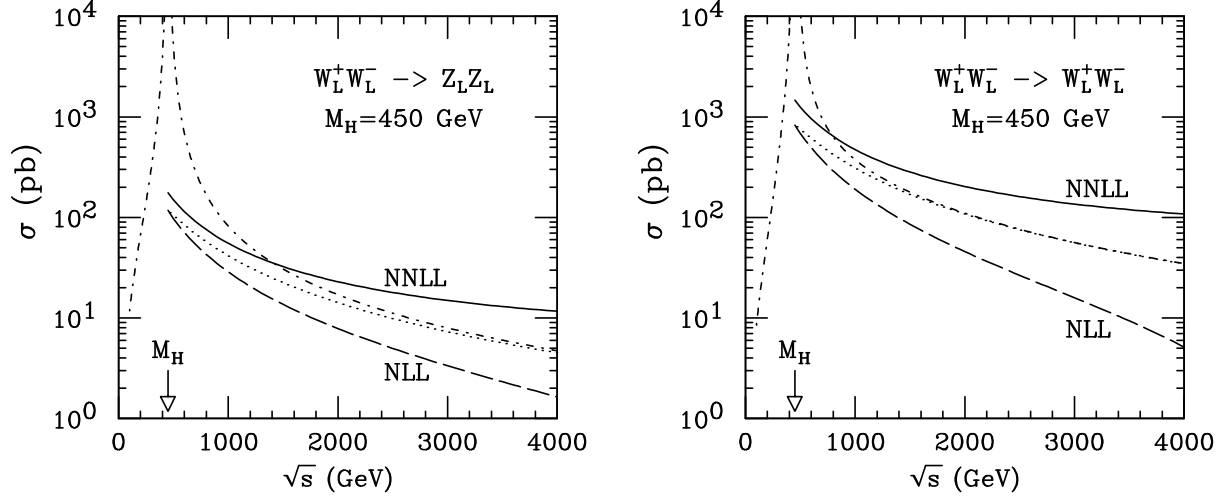


FIG. 7. Left plot: The cross section of the process $W_L^+ W_L^- \rightarrow Z_L Z_L$ as a function of the cms-scattering energy \sqrt{s} for $M_H = 450$ GeV. We show the NLL and NNLL curves of Fig. 5, now for the whole range $M_H < \sqrt{s} < 4000$ GeV, using a logarithmic scale for the cross section. In addition, we show the exact one-loop cross section (dot-dashed curve) and the high-energy one-loop cross section (dotted curve), both without resummation of logarithms. The large corrections to the high-energy cross section change the exact cross section significantly, introducing large uncertainties for $\sqrt{s} > 2M_H$. For $\sqrt{s} \gtrsim 1500$ GeV even the NNLL perturbative result is not expected to be reliable anymore: perturbation theory fails. Right plot: The cross section of the process $W_L^+ W_L^- \rightarrow W_L^+ W_L^-$ as a function of the cms-scattering energy \sqrt{s} for $M_H = 450$ GeV. The curves have the same meaning as in the left plot, and the same conclusions apply.